The abortive SARS-CoV-2 infection of osteoclast precursors promotes their differentiation into osteoclasts

SVIERCZ Franco[¤1], JARMOLUK Patricio[¤1], GODOY COTO Joshua[2], CEVALLOS Cintia[1], FREIBERGER Rosa Nicole[1], LÓPEZ Cinthya Alicia Marcela[1], ENNIS Irene Lucia[2], DELPINO M. Victoria[1], QUARLERI Jorge[1*]

[1]Universidad de Buenos Aires (UBA), Consejo de Investigaciones Científicas y Técnicas (CONICET), Instituto de Investigaciones Biomédicas en Retrovirus y Sida (INBIRS), Paraguay 2155, piso 11, Buenos Aires C1121 ABG, Argentina.

[2]Universidad Nacional de la Plata (UNLP), Consejo de Investigaciones Científicas y Técnicas (CONICET), Centro de Investigaciones Cardiovasculares "Dr. Horacio E. Cingolani", La Plata, Buenos Aires, Argentina.

*Correspondence: quarleri@fmed.uba.ar

[¤] These two authors contributed equally to this work

List of authors

-Sviercz F., M.Sc. francosviercz@gmail.com

-Jarmoluk P., M.D. patriciojarmoluk@gmail.com

-Godoy Coto J., M.Sc. joshuagodoycoto@gmail.com

-Cevallos C., Ph.D. cevalloscintia@gmail.com

-Freiberger R. N. M.Sc. freibergernicole@gmail.com

-López C. A. M. M.Sc. alilopez1996@gmail.com

-Ennis I.L., MD, Ph.D. iennis@med.unlp.edu.ar

-Delpino M.V., Ph.D. mdelpino@ffyb.uba.ar

-Quarleri J., Ph.D. quarleri@fmed.uba.ar 0000-0001-5110-8773

Running head: SARS-CoV-2 promotes osteoclastogenesis

ABSTRACT

The COVID-19 pandemic has resulted in the loss of millions of lives, although a majority of those infected have managed to survive. Consequently, a set of outcomes, identified as long COVID, is now emerging. While the primary target of SARS-CoV-2 is the respiratory system, the impact of COVID-19 extends to various body parts, including the bone. This study aims to investigate the effects of acute SARS-CoV-2 infection on osteoclastogenesis, utilizing both ancestral and Omicron viral strains. Monocyte-derived macrophages (MDM), which serve as precursors to osteoclasts, were exposed to both viral variants. However, the infection proved abortive, even though ACE2 receptor expression increased post-infection, with no significant impact on cellular viability and redox balance. Both SARS-CoV-2 strains heightened osteoclast formation in a dose-dependent manner, as well as CD51/61 expression and bone resorptive ability. Notably, SARS-CoV-2 induced early pro-inflammatory M1 macrophage polarization, shifting towards an M2-like profile. Osteoclastogenesis-related genes (RANK, NFATc1, DC-STAMP, MMP9) were upregulated, and surprisingly, SARS-CoV-2 variants promoted RANKL-independent osteoclast formation. This thorough investigation illuminates the intricate interplay between SARS-CoV-2 and osteoclast precursors, suggesting potential implications for bone homeostasis and opening new avenues for therapeutic exploration in COVID-19.

KEYWORDS: SARS-CoV-2; COVID-19; osteoclasts; bone; monocyte-derived macrophages; RANKL.

1. Introduction

Coronavirus Disease 2019 (COVID-19), caused by severe acute respiratory syndrome coronavirus 2 (SARS-CoV-2), leads to severe cases and long-term complications, including multi-organ dysfunction(1-7). Post-recovery focuses on respiratory, cardiac, and neurological functions, neglecting potential skeletal issues. Older patients with comorbidities and medication use may suffer unnoticed impacts on bone health.

While the diverse clinical symptoms of COVID-19 are well-documented, the degenerative changes in the skeletal system induced by SARS-CoV-2 remain underexplored. Up to 24% of long-term COVID patients reported persisting bone pain or burning for seven months post-infection(8). Interestingly, non-intensive care COVID-19 patients exhibited significantly higher bone mineral density (BMD) than those in critical care(9).

Bone remodeling is a pivotal and ongoing process for maintaining bone balance, relying on the coordination of osteoblasts and osteoclasts guided by osteocytes(10). Osteoclasts (OC), specific to bone tissue, originate from monocyte/macrophage-derived precursors influenced by macrophage colony-stimulating factor (M-CSF) and receptor activator nuclear factor kappa B ligand (RANKL). The formation of osteoclasts involves the fusion of mononucleated precursors. The process of bone resorption, facilitated by integrins such as the CD51/61 vitronectin receptor, encompasses matrix metalloproteinases (MMPs) produced by OC(10-12).

During viral infections, osteoclasts, targeted by microorganisms, undergo significant activation, leading to bone loss. In the case of HIV infection, bone resorption is promoted, with the extent influenced by the infection load(13, 14). On the other hand, Zika virus infection impedes bone remodeling in osteoclasts(15). Research utilizing animal models suggests that SARS-CoV-2 affects bone metabolism both during acute infection and in the post-recovery phases(16-18).

This study examines the direct effects of SARS-CoV-2 on osteoclastogenesis, maturation, and resorption activity using osteoclast precursors from human peripheral blood mononuclear cells. Two SARS-CoV-2 strains were evaluated for their differential effects on OC differentiation and osteoclastogenesis. Results indicate that even in the absence of productive infection, SARS-CoV-2 exposure accelerates osteoclastogenesis, bone loss, and resorption at various stages of OC differentiation.

2. Material and Methods

Monocytes-derived macrophage culture and differentiation to osteoclasts. Human monocytes were isolated from the blood of anonymous healthy donors and differentiated as monocyte-derived macrophages (MDM), as described previously (14). Briefly, monocytes were seeded on slides in 24-well plates at a density of 5×10^5 cells/mL in RPMI medium (Gibco) supplemented with 10% heat-inactivated fetal bovine serum (FBS) (Sigma-Aldrich), 2 mM of L-glutamine (Gibco), 1 mM of sodium pyruvate (Gibco), penicillin-streptomycin (Sigma-Aldrich) and M-CSF (10ng/mL) (StemCell Technologies) for 6 days. Then, mature osteoclasts (OC) were obtained from cultured MDM (osteoclast precursors) in alpha minimum essential medium (α-MEM) (Gibco) supplemented with 10 % FBS, 2mM of L-glutamine (Gibco), 1mM of sodium pyruvate (Gibco), and penicillin-streptomycin (α-MEM complete medium), M-CSF (10ng/mL) and RANKL (30ng/mL) (StemCell Technologies) for 9 days (mature osteoclast).

Ethical approval for this study was granted by the institutional review board and local ethical committee (Number: RESCD-2023-872). Buffy coats from healthy donors, aged 18 to 60 with a balanced gender ratio, were sourced from Hospital de Clínicas ‘‘José de San Martín’’, Facultad

de Medicina, Universidad de Buenos Aires. All human samples, obtained regardless of this study, were provided without personally identifiable information.

Virus. SARS-CoV-2 ancestral (Wh) strain was provided by Dr. Sandra Gallego (Universidad Nacional de Córdoba, Argentina), and the Omicron (BA.5) strain was obtained from a nasopharyngeal swab, characterized and then propagated, and titrated in African green monkey kidney cell line Vero cells (2.85×10^6 TCID50 per ml). The Vero E6 (ATCC, Rockville, MD) was cultured as monolayers in a 5% CO_2 atmosphere at 37°C in DMEM (Sigma-Aldrich, Argentina) supplemented with 2mM L-glutamine, 10% FBS (Sigma-Aldrich, Argentina), 100U/mL penicillin and 100µg/mL streptomycin.
In 24-well plates, 5×10^5 MDM/mL in RPMI (Gibco) were cultured in RPMI complete medium with M-CSF (10ng/mL; StemCell Technologies) for 3 days and separately infected with the two studied SARS-CoV-2 variants using a MOI=0.1. When appropriate, MOI=0.01 and 1.0 were also used. The infection occurred in RPMI without FBS for 4 hours, followed by 4-5 washes with PBS 1X (the last wash serving as T0), and a complete RPMI medium with M-CSF (10ng/mL) was added. Finally, at 3 days post-infection (dpi), α-MEM complete medium with M-CSF (10ng/mL) with or without RANKL (30ng/mL) was added.

Detection and quantification of SARS-CoV-2 genomic RNA. RNA was extracted from both, cells and culture supernatants using Chemagic™ Viral DNA/RNA kit special H96 on the automated Chemagic™ 360 instrument (PerkinElmer). RNA was quantified using a NanoDrop™ (Thermo Scientific) and its load was normalized before SARS-CoV-2 RNA detection was performed using RT-qPCR (DisCoVery SARS-CoV-2 RT-PCR Detection Kit Rox) amplifying ORF1ab and N viral genes following the manufacturer's instructions.
In culture supernatants, viral load was calculated by interpolation of the corresponding Ct value with a standard curve, which had been built with the Ct values obtained following PCR amplification of samples containing serial dilutions of quantified SARS-CoV-2 positive RNA control (GISAID EPI_ISL_420600). In cell lysates viral load was normalized to human RNAse P gene and expressed as $2^{-\Delta ct}$.

Titration of SARS-CoV-2 infectious particles. The release of infectious viral particles into the supernatant was assessed using Vero E6 cells. Briefly, Vero cells were seeded in 96-well plates, and the culture supernatants to be tested were added for 1 h at 37°C. Afterward, the supernatant was removed, and DMEM with 2% FBS was added. Plates were then incubated for 3 days at 37°C. The infectious titer of each supernatant was determined by TCID50 and expressed as plaque-forming units (PFU) per mL.

Flow cytometry analysis. Cells detached using Accutase® (StemCell Technologies) were stained for surface antigens for 30 minutes at 4°C. To characterize the macrophage activation profile, anti-human CD80, anti-human CD206, and anti-human CD163 were employed. The osteoclast-specific CD51/61 marker was measured using an anti-CD51/61-FITC antibody. The ACE2 expression was quantified using a rabbit primary polyclonal antibody to human-ACE2. The determination of intracellular SARS-CoV-2 nucleocapsid was performed on fixed and permeabilized cells with Fixation/Permeabilization Kit (BD Biosciences) according to the manufacturer's using a rabbit primary antibody to nucleocapsid. The Goat Anti-Rabbit IgG secondary polyclonal antibody was used. For further information on antibodies used in flow cytometry see Supplementary Table 1.

Cell death percentage was assessed using APC-conjugated annexin-V and 7-AAD staining with the apoptosis detection kit (BD Biosciences). Freeze-thaw cycles served as a positive control for cell death. Mitochondrial reactive oxygen species (mROS) were measured using 5 μM MitoSOX™ (Thermo Fisher Scientific) staining for 30 min. Data were acquired using Full Spectrum Flow Cytometry Cytek® Northern Lights 3000™ (Cytek Biosciences Inc.) and analyzed with FlowJo.v10.6.2 (Ashland).

Western Blot. Macrophages ($5x10^5$) were sonicated in RIPA buffer (Santa Cruz Biotechnology, sc-29498) with protease inhibitors cocktail (Roche). Protein concentration was determined by the Bradford method (Bio-Rad dye reagent) as described by the manufacturer with BSA as standard. Equal amounts of protein per lane were run in an SDS-PAGE and then electrotransferred to PVDF membranes. Membranes were blocked with 5% non-fat milk for 1 hour and incubated overnight with a specific antibody against ACE2 (PA5-20040, Thermo Fisher). Anti-Na+/K+ ATPase (Thermo Fisher, MA532184) was used as a loading control. Peroxidase conjugated anti-rabbit (NA934, GE Healthcare Life Sciences) was used as the secondary antibody. Bands were visualized with enhanced chemiluminescence reagent (ECL, Millipore) and a Chemidoc Station (Bio-Rad) and quantified using Image Lab software (Bio-Rad).

Assessment of osteoclast differentiation. Cells were fixed with PFA 4% and stained for evaluating the generation of mature multinucleated osteoclasts using Tartrate Resistant Acid Phosphatase (TRAP) (Sigma-Aldrich, USA) according to the manufacturer's protocol. Briefly, at the end of the experimental timeline cells were washed twice with 1XPBS and fixed with a fixative solution comprised of citrate, acetone, and 4% formaldehyde for 10 min at 37°C. After washing twice with 1XPBS, fixed cells were stained for TRAP at 37°C in the dark for 1 hour. Multinucleated TRAP-positive cells with ≥ 3 nuclei were considered mature osteoclasts. TRAP-positive multinucleated cells were further counted and imaged using an inverted microscope 200x (ECLIPSE, TS100, Nikon).

Measurement of TNF-α, IL-6, and IL-1β concentration. TNF-α, IL-6, and IL-1β were measured by sandwich ELISA in culture supernatants using paired cytokine-specific monoclonal antibodies, according to the manufacturer's instructions (BD Pharmingen).

Quantitative real-time PCR. Quantitative RQ-PCR was utilized to detect the gene expression of M1 and M2-related cytokines as well as key regulators of osteoclast differentiation. Total RNA was isolated using a GenElute™ Total RNA isolation kit from Sigma-Aldrich, and RNA quantification was performed on a nanodrop spectrophotometer. cDNA was synthesized using the ImPromII Reverse Transcription System (Promega). Real-time PCR was conducted on a StepOne PCR system (Applied Biosystems) with SYBR green for PCR product detection. Cycling conditions and primers' sequences for various target genes, including GAPDH, IL-10, TGF-β, TNF-α, IL-1β, NFATc1, DC-STAMP, MMP-9, and RANK. For primer sequences and cycling conditions see Supplementary Table 2.
The fold-change (relative expression) in gene expression was calculated using the relative quantification method ($2^{-\Delta\Delta Ct}$)(19). Relative expression levels were normalized against GAPDH. Intra-experiment CT value differences between samples were less than 0.5.

Assessment of bone resorption. To assess bone resorption activity, macrophages were seeded on bovine cortical bone slices (Boneslices, Inc.) and differentiated into osteoclasts. Following complete cell removal by several washes with water, bone slices were stained with toluidin blue

(Sigma-Aldrich) to detect resorption pits under a light microscope (ECLIPSE, TS100, Nikon). The surface of bone degradation areas was quantified manually with ImageJ software (version 1.47).

Statistical Analysis.

The figure legends provide the exact values of n (donors). For datasets with a normal distribution (confirmed by the Kolmogorov-Smirnov test), two-tailed paired or unpaired t-tests were employed. Alternatively, two-tailed Mann-Whitney (unpaired test) or Wilcoxon matched-paired signed rank tests were applied, using GraphPad Prism 7.0 (GraphPad Software Inc.). A significance level of $p < 0.05$ was considered (*$p \leq 0.05$; **$p \leq 0.01$; ***$p \leq 0.001$, ****$p \leq 0.0001$).

3. Results

3.1 SARS-CoV-2 causes an abortive infection in osteoclast precursors during their differentiation.

The experimental timeline, outlined in Figure 1A, involved separately exposing monocyte-derived macrophages (MDM) to each of the two studied SARS-CoV-2 variants (ancestral and Omicron). Remarkably, comparable viral infection kinetics were observed even during MDM differentiation into osteoclasts, as illustrated in Figure 1B. The assessment, conducted at 3, 6, 9, and 12 days post-infection (dpi), included measuring viral load in cell supernatants (via RT-qPCR) and intracytoplasmic viral load in cell lysates. In addition, infection efficiency was evaluated through flow cytometry, measuring the relative abundance of intracellular nucleocapsid protein (N)-expressing cells. The viral load in MDM culture supernatants for each SARS-CoV-2 variant, measured using both N-gene and ORF-1a-gene, exhibited an initial increase from inoculation to 3 dpi, followed by a progressive decline at 6, 9, and up to 12 dpi (Figure 1B). Contrarily, intracytoplasmic RNA in cell lysates, measured using both N-gene and ORF-1a-gene, exhibited a progressive decrease from inoculation to 12 dpi (Figure 1C). The undetectable levels (%) of the SARS-CoV-2 capsid protein (N) were found for both variants at 3 dpi by flow cytometry (Figure 1D).

Furthermore, an assay to detect infective viral particles in supernatants for the SARS-CoV-2 ancestral strain revealed undetectable de novo production of viral particles from the infectious inoculum to 72 hpi (Figure 1E).

In summary, after exposure to SARS-CoV-2 (Wh and BA.5 strains), abortive infections were observed in MDM both before and during their differentiation into osteoclasts, highlighting the intricate dynamics of viral replication and host response throughout the experimental timeline.

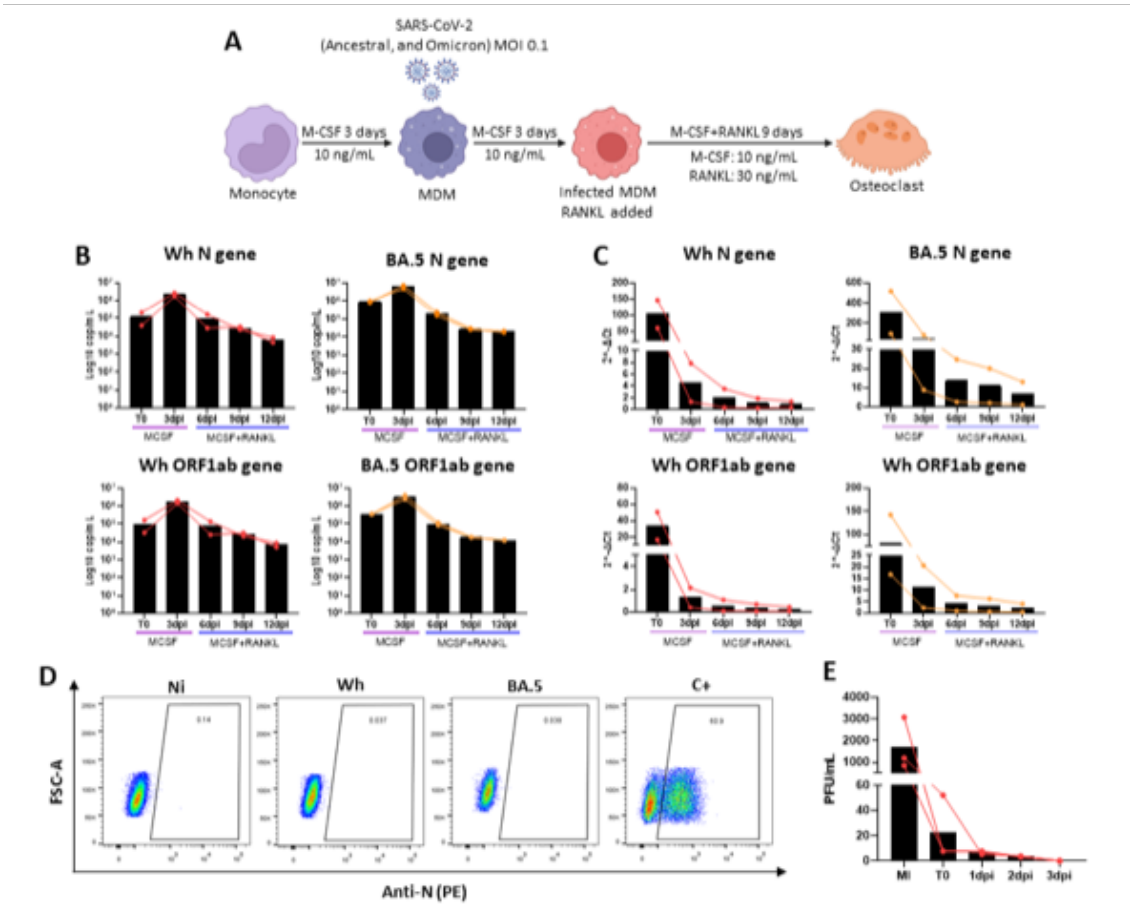

Figure 1. **SARS-CoV-2 replication kinetics**.**(A)** Representation of the experimental timeline schedule.**(B)** Kinetics of SARS-CoV-2 replication using ancestral (Wh; left) and Omicron (BA.5; right) measured by mRNA of nucleocapsid (top) and ORF1ab (bottom) in culture supernatants via qPCR during osteoclast formation. **(C)** Kinetics of SARS-CoV-2 replication using ancestral (Wh; left) and Omicron (BA.5; right) measured by mRNA of nucleocapsid (top) and ORF1 (bottom) intracellularly in cell lysates via qPCR during osteoclast formation (normalized to human RNase P gene).**(D)** The efficiency of SARS-CoV-2 infection (measured by flow cytometry as intracellular expression of viral nucleocapsid) at 3 dpi; expression in the infected VeroE6 cell line was used as a positive control. (E) SARS-CoV-2 (Wh strain) titration in culture supernatants reported as the number of plaque-forming units per ml (PFU/ml). dpi, days post-infection. n: 2-5 donors were used.

3.2 Cell viability and redox balance are preserved when macrophages are abortively infected by SARS-CoV-2

Even when the infection is abortive it might trigger macrophage activation and several biochemical and morphological changes leading to programmed cell death (20). Thus, to ensure that cellular-related parameters are comparable between virus-infected and control groups, the level of programmed cell death was measured.

As shown in Figures 2A and 2B, cell viability (%) remained preserved among macrophages after SARS-CoV-2 exposure from 3 dpi and throughout osteoclastogenesis until 12 dpi.

Reactive oxygen species (ROS) production increases during M-CSF-induced macrophage differentiation from monocytes and they are mainly produced by mitochondria (mROS)(21). It may influence osteoclast differentiation. As depicted in Figures 2C and 2D, cellular mROS levels (%) were assessed post SARS-CoV-2 infection before RANKL treatment. A slight increase in mROS

production was observed immediately after virus-cell contact, but no significant differences were evident during the follow-up at 4, 24, and 72 hpi.

Taken together, both cell viability and mROS levels were maintained under the experimental conditions before and after the SARS-CoV-2 challenge.

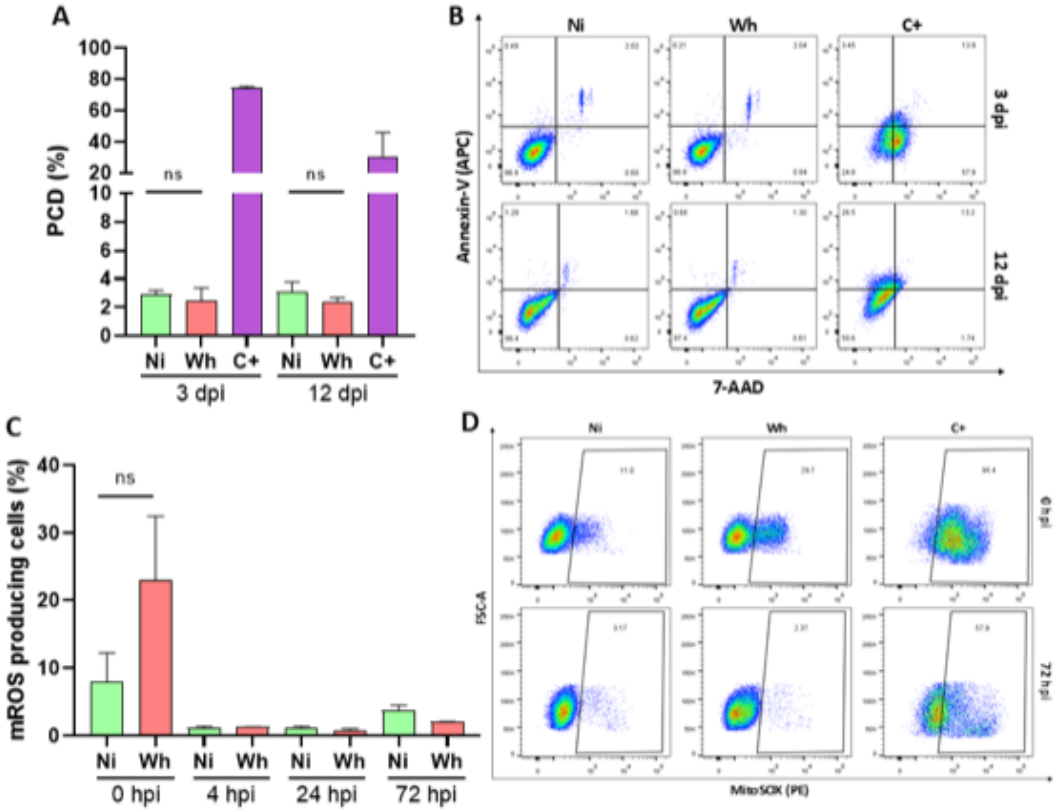

Figure 2. Effects of SARS-CoV-2 on cell viability and mROS production. (A) Assessment of programmed cell death, presented as the percentage of cells stained with Annexin V/7-AAD, following SARS-CoV-2 infection with the ancestral variant at two distinct time points, 3 dpi and 12 dpi. **(B)** Representative dot plots obtained through flow cytometry, illustrating Annexin V/7-AAD staining at the time points indicated in (A). **(C)** Quantification of mitochondrial ROS (mROS) production, expressed as the percentage of cells stained with MitoSOX measured by flow cytometry, at various time intervals. **(D)** Representative dot plots for cellular mROS measurement obtained through flow cytometry, illustrating MitoSOX staining at the time points indicated in (C). Wh, ancestral variant. Ni, non-infected controls. hpi, hours post-infection. ns = not significant. n: 2-5 donors were used.

3.3 SARS-CoV-2 induces upregulation of ACE2 expression in macrophages

Given that ACE2 serves as the primary receptor for SARS-CoV-2, the level of its expression on macrophages delineates susceptibility to infection and replication. Moreover, the potential viral-induced impact on its expression was also assessed. This investigation involved a comprehensive analysis employing two distinct technical approaches. First, the expression level of ACE2 in MDMs using flow cytometry after 3-days of infection was examined. As shown in Figures 3A and 3B, the analysis revealed that ACE2 was expressed in low frequency (4.7±1.6 %) in control cells. However, among SARS-CoV-2–infected MDMs from the same donors, a significantly increased level of ACE2 expression was measured (Wh: 10.5±4.1%; $p<0.05$). Second, ACE2 protein expression measured by western blotting from MDM homogenates revealed that these osteoclast precursors infected with SARS-CoV-2 had a significant increase (3.5-fold-change; $p<0.01$) in receptor expression compared with control-MDM (Figures 3C, 3D).

These results demonstrate that MDM express the ACE2 receptor at a low level, which is upregulated after the SARS-CoV-2 challenge.

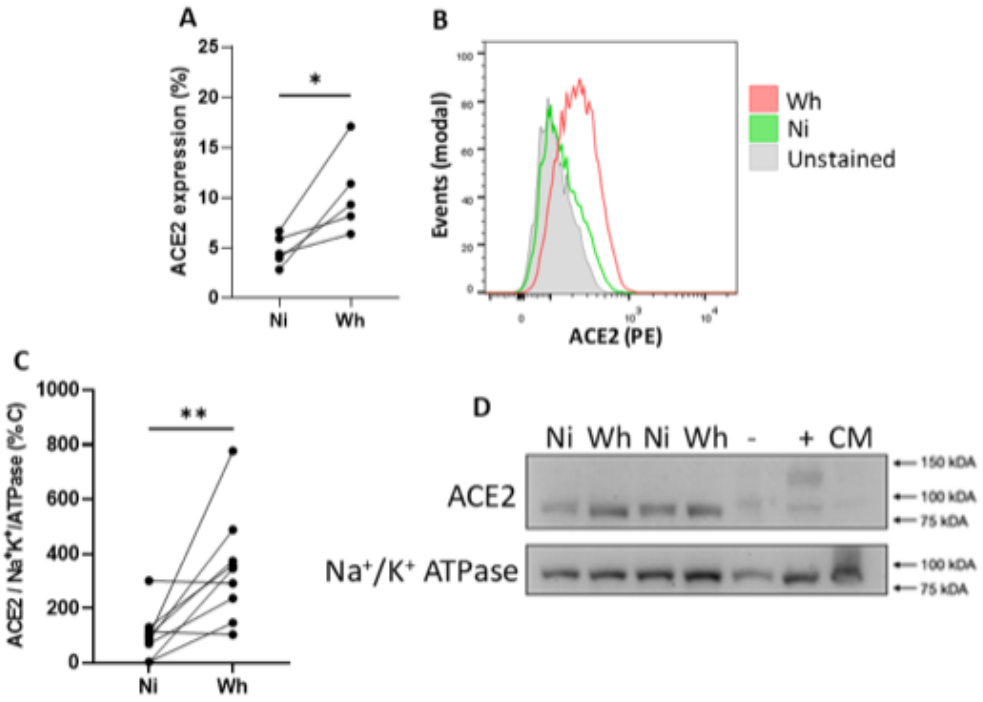

Figure 3. SARS-CoV-2 increases ACE2 expression in infected macrophages. (A) Evaluation of ACE2 surface expression in macrophages at 3 dpi, measured through flow cytometry (values connected are paired samples obtained from the same donor). **(B)** Representative histograms obtained by flow cytometry illustrating ACE2 expression as depicted in (A). **(C)** Quantification of relative ACE2 protein expression via Western blot analysis. Values connected are paired samples obtained from the same donor. **(D)** Representative blots of ACE2 and Na+/K+ ATPase. Wh, ancestral variant. Ni, non-infected controls. —: Jurkat cells; +: Huh7.5 cells, CM: cardiomyocytes, n: 5-8 donors were used.

3.4 OC formation is enhanced by ancestral and Omicron SARS-CoV-2 strains in a dose-dependent manner

To determine the influence of SARS-CoV2 in osteoclastogenesis, human MDM (from 4-5 donors) were exposed to two viral variants, (Wh, BA.5). At 12-dpi, osteoclast formation in culture was quantified and its relative abundance (%±SD) was calculated after manually counting TRAP-positive, multinucleated (≥3 nuclei) cells visualized under the microscope (x200). As shown in Figures 4A and 4B, MDM exposure to Wh or BA.5 virus strain triggered significantly higher MDM fusion into osteoclasts compared to non-infected cells (Ctrl:5.5±1; Wh:9.6±1.2; BA.5:10.1±2%). Moreover, for both viral variants, SARS-CoV2-enhanced osteoclastogenesis depicts an inoculum dose response. As shown in Figures 4C and 4D, when MDM were exposed to a ten-fold increased viral inoculum (MOI 0.01→0.1→1.0), the abundance of OC (%) was significantly higher for both, ancestral (6.3±2.3→9.0±1.2→10.0±1.4) and Omicron (7.2±1.1→9.7±1.0→10.5±0.5) strain.

These findings show that osteoclast formation is significantly boosted in a dose-dependent manner when its precursors are abortively infected by SARS-CoV-2.

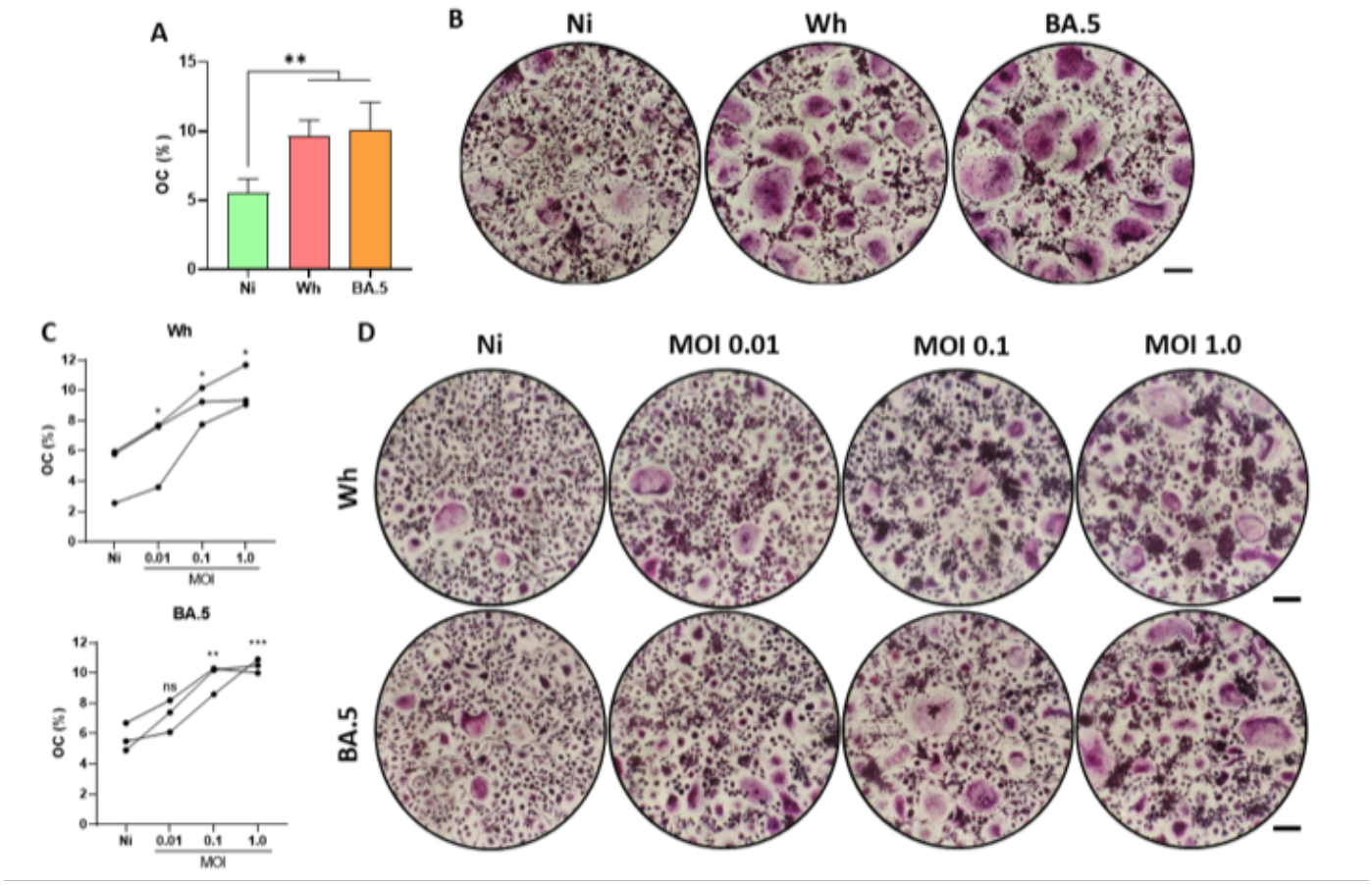

Figure 4. SARS-CoV-2 positively modulates osteoclast differentiation. (A) Osteoclast quantification presented as a percentage (%) of OC/total cells at 12 dpi. **(B)** Representative images corresponding to (A) at 200x magnification. **(C)** Osteoclast quantification displayed as a percentage (%) of OC/total cells at 12 dpi, infected with three different multiplicities of infection (MOI). Values connected are paired samples obtained from the same donor. **(D)** Representative images corresponding to (C) at 200x magnification. Ni, non-infected controls. Wh, ancestral variant. BA.5, Omicron variant. Scale bar: 200 µm. *p < 0.05, **p < 0.01, and ***p < 0.001. ns, not significant. n: 2-5 donors were used.

3.5 Osteoclasts CD51/61 expression and resorptive ability is up-modulated by SARS-CoV-2

The integrin complex CD51/CD61, also known as αVβ3, is expressed at high levels on osteoclasts. The SARS-CoV2 influence on the CD51/61 expression was evaluated. Besides their morphology and TRAP expression, this marker is expressed in differentiated osteoclasts as a receptor for vitronectin. Figures 5A and 5B show that, after 9-days of osteoclastogenesis with M-CSF+RANKL (12 dpi), a significantly higher level of CD51/61 expression (%) was measured when OC precursors were exposed to SARS-CoV2 (Ctrl:20.7±9.2; Wh:30.7±14.0).

To assess the impact of SARS-CoV-2 on osteoclastogenesis and subsequent resorptive ability, infected osteoclast precursors were cultured on bone slices and differentiated into mature osteoclasts by RANKL for 9 days. Figures 5C and 5D illustrate the defined resorption pits, showing significantly greater osteoclast activity in SARS-CoV-2-exposed cultures ($p<0.05$). The resorbed bone area (%) was markedly increased compared to control (Ctrl: 10.7±1.1; Wh:22.2±2.1; BA.5: 20.4±2.4). These findings highlight the SARS-CoV-2-mediated upregulation of CD51/61 expression among osteoclasts, which would facilitate interactions with the extracellular matrix,

cell adhesion, and bone resorption. In line, both SARS-CoV-2 strains can increase osteoclast traits, such as multinuclearity and bone resorption competence.

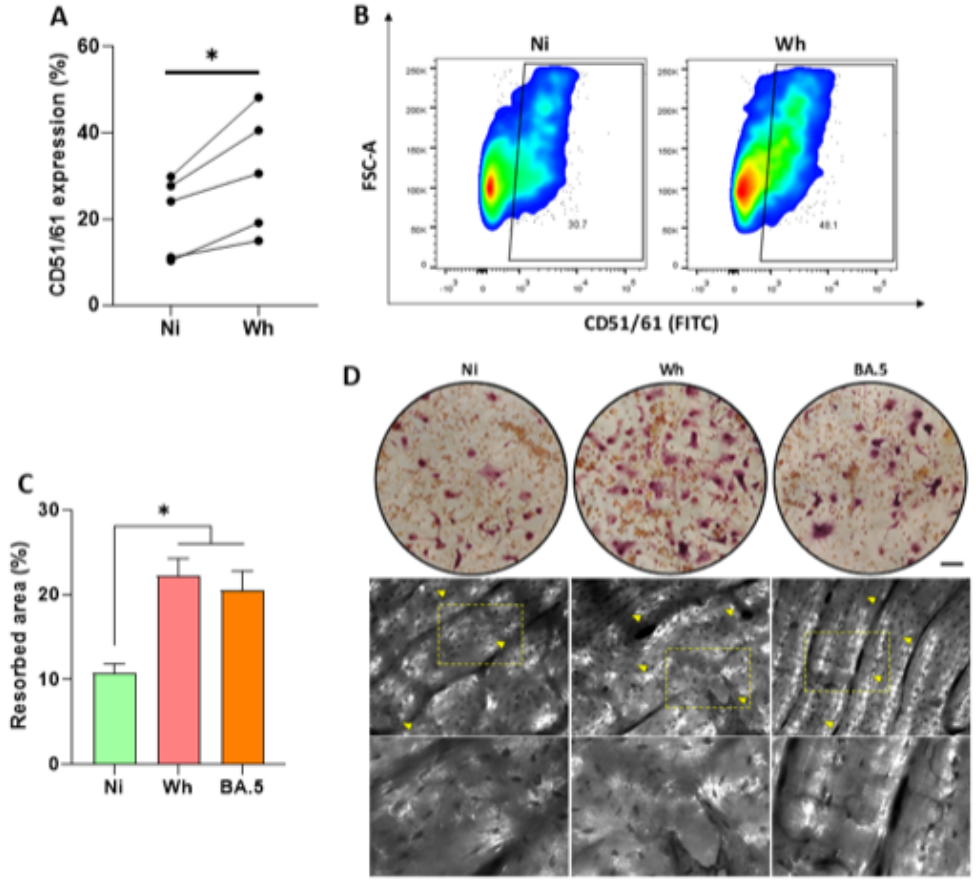

Figure 5. SARS-CoV-2 enhances osteoclast maturation and bone-resorbing activity. (A) CD51/61 expression in osteoclasts at 12 dpi, measured by flow cytometry (values connected are paired samples obtained from the same donor). **(B)** Representative dot plots obtained by flow cytometry depicting CD51/61 expression (A). **(C)** Resorption area expressed as a percentage of the total analyzed field observed under a light microscope (200x magnification) and analyzed using Image-J. **(D)** Top: Representative data of TRAP-positive (red) osteoclasts at 12 dpi. Bottom: Bone resorption pits formed by osteoclasts, staining slices at 12 dpi with toluidine blue. Yellow arrowheads indicate the presence of pits. Zoomed-in views of yellow dashed squares provide a more detailed observation. Ni, non-infected controls. Wh, ancestral variant. BA.5, Omicron variant. Scale bar: 200 µm. *p < 0.05. n: 2-3 donors were used.

3.6 RANK, NFATc1, DC-STAMP, and MMP9 mRNA levels are differently regulated during osteoclastogenesis in response to infection

The SARS-CoV-2 influence on different osteoclastogenesis-related genes was evaluated. The RANKL and its receptor RANK play critical roles in controlling the development, activation, and survival of osteoclasts. As shown in Figure 6A, at 3dpi the RANK mRNA level in infected macrophages was higher than non-infected control (7.5-fold-change). According to the timeline, at 3 dpi the macrophages are exposed to RANKL activating other signals involved in differentiation and fusion. As the RANK/RANKL interaction triggers NFATc1 transcription, a master regulator of osteoclast differentiation, its mRNA level post-RANKL stimulus at 6 dpi was measured. As presented in Figure 6B, the mRNA levels in infected cultures were significantly elevated compared to those Ctrl (7.4-fold-change). Additionally, mRNA levels of DC-STAMP, a

surface receptor necessary for osteoclast fusion, and MMP9, a collagenase abundantly expressed in osteoclasts, were examined at 12 dpi. As illustrated in Figures 6C and 6D, both DC-STAMP and MMP9 mRNA were notably increased in cells exposed to SARS-CoV-2 (1.9 and 2.5-fold-change respectively).
Thus, the mechanism of the SARS-CoV-2-enhanced osteoclast differentiation includes the RANK/RANKL pathway, resulting in increased expression of NFATc1, DC-STAMP, and MMP9.

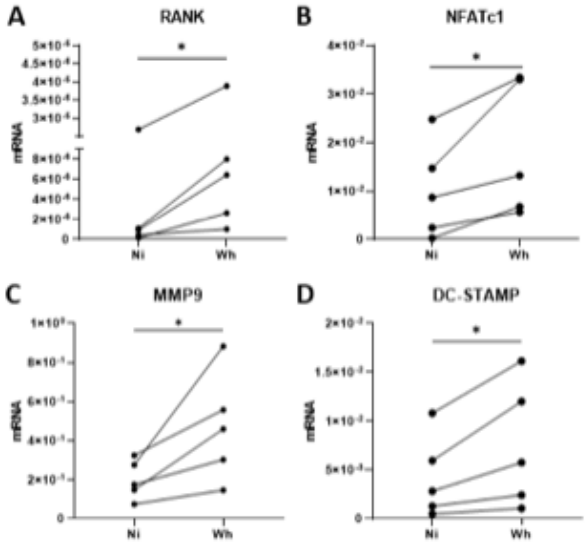

Figure 6. mRNA Levels of RANK, NFATc1, MMP9, and DC-STAMP during osteoclastogenesis after SARS-CoV-2 infection. The mRNA levels (expressed as $2^{-\Delta Ct}$) of: **(A)** RANK at 3 dpi, **(B)** NFATc1 at 6 dpi, **(C)** MMP9 at 12 dpi, and **(D)** DC-STAMP at 12 dpi, were quantified using real-time quantitative PCR (RQ-PCR) in paired samples obtained from the same donor. The values of mRNA levels are relative to GAPDH (a housekeeping gene). Ni, non-infected controls. Wh, ancestral variant. *$p < 0.05$. n: 4-6 donors were used.

3.7 SARS-CoV-2 drives early pro-inflammatory M1 macrophage polarization shifting towards an M2-like profile during infection.

To analyze the impact of SARS-CoV-2 on macrophage activation during osteoclast differentiation, a three-day exposure to the virus was conducted before RANKL treatment. As shown in Figure 7A, at 1 and 3 dpi, non-infected macrophages predominantly appeared as small, roundish cells. SARS-CoV-2-infected macrophages exhibited mainly amoeboid morphology, while at 3 dpi, roundish and amoeboid macrophages, as well as large bipolar spindeloid macrophages, were observed, resembling M1 and M2-like phenotypes, respectively. Phenotypically these cells revealed early increases in CD80 (M1 marker) at 1 dpi and comparable CD206 levels (M2 marker) in infected macrophages compared to non-infected controls but lower CD163 levels (M1 to M2 shifting marker) were observed. Then, among SARS-CoV-2-infected cells, CD80 decreased, CD206 and CD163 increased at 2 dpi, and later (3 dpi), CD80 levels normalized, while CD206 and CD163 peaked in virus-infected cultures (Figure 7B, 7C). Pro-inflammatory cytokines, significantly increased in SARS-CoV-2 infected macrophages compared to undetectable or very low levels in controls, were observed with TNF-α peaking at 1 dpi, IL-1β at 2 dpi, and constant IL-6 levels (Figure 7D). Figure 7E presents results obtained by RT-qPCR at 3 dpi, indicating the upregulation of M2-related cytokine mRNA (TGF-β and IL-10: 6.7 and 4.2-

fold change, respectively) and TNF-α (2.5-fold change), but not IL-1β (1.1-fold change). Collectively, the abortive infection by SARS-CoV-2 initiates an early M1-like activation profile, transitioning to an M2-like state, as indicated by altered cell surface markers and cytokine production patterns.

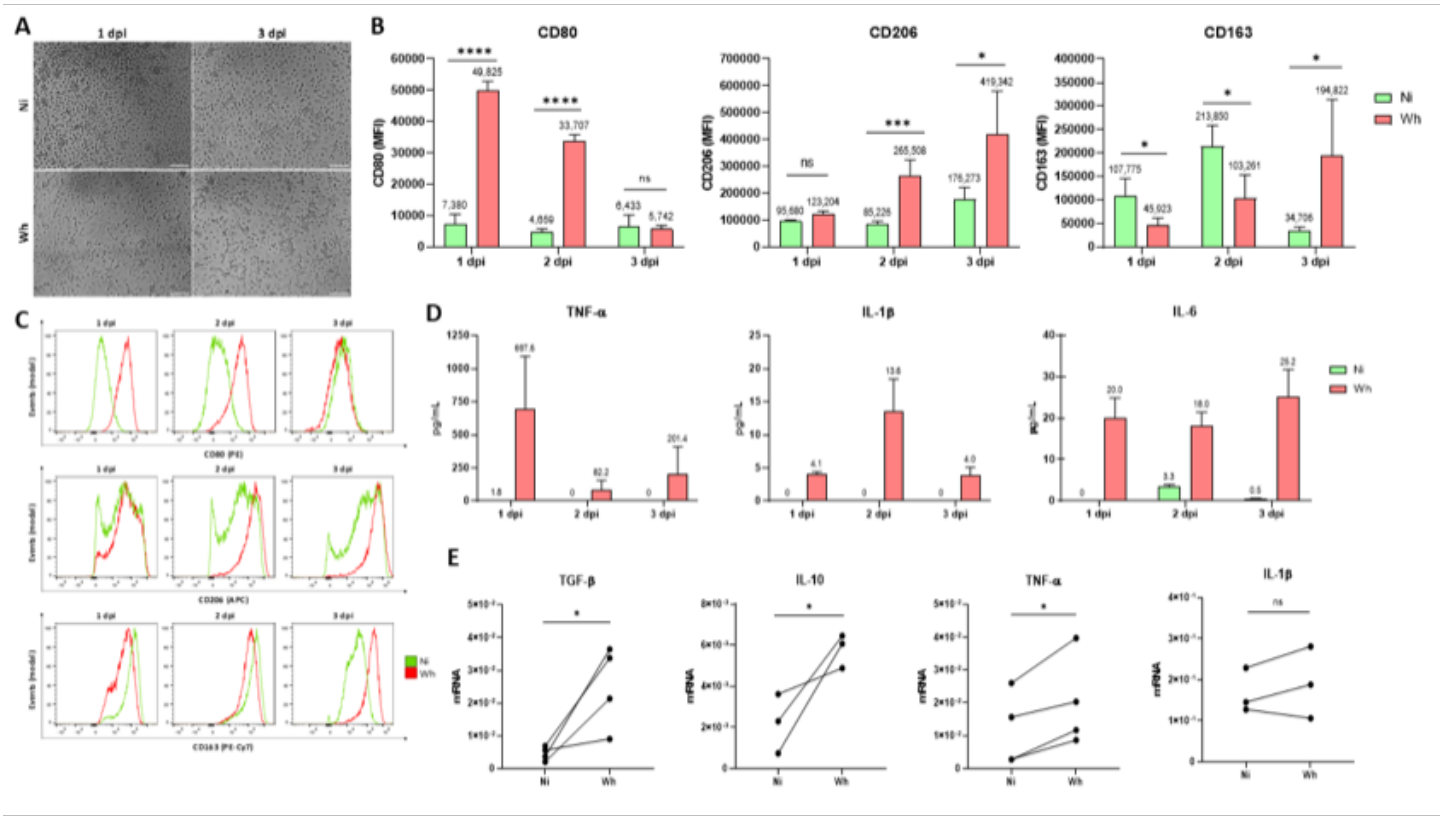

Figure 7. SARS-CoV-2 infection of macrophages induces a profile switch from M1 to M2. (A) Representative images of macrophage morphology at two different time points, 1 dpi, and 3 dpi (100x). Scale bar 50 µm. **(B)** Kinetics of membrane cell markers of M1 and M2 macrophages measured by flow cytometry during SARS-CoV-2 infection. Mean fluorescence intensity (MFI) median values are shown. **(C)** Representative histograms of flow cytometry in (B). **(D)** Kinetics of cytokines production in cell supernatants measured by ELISA during SARS-CoV-2 infection. **(E)** Measurement of mRNA of M2-related cytokines (TGF-β and IL-10) and M1-related cytokines (TNF-α and IL-1β) by RT-qPCR at 3 dpi in paired samples obtained from the same donor. The values of mRNA levels are relative to GAPDH (a housekeeping gene). Ni, non-infected controls. Wh, ancestral variant. *p < 0.05. **p < 0.01. ***p < 0.001. ****p < 0.0001. ns = not significant. n: 5-8 donors were used.

3.8 SARS-CoV-2 variants promote RANKL-independent osteoclast formation

To ascertain whether the early pro-inflammatory environment induced by SARS-CoV-2 could prompt the differentiation of macrophages into osteoclasts, MDM were exposed to two viral variants (Wh, BA.5) and maintained in a media with MCSF alone in the absence of RANKL. At 12 dpi, osteoclast formation in culture was quantified by manually counting TRAP-positive, multinucleated (≥3 nuclei) cells visualized under the microscope (x200; mean number ± SD). As depicted in Figures 8A and 8B, exposure of MDM to the ancestral or BA.5 virus strains resulted

in a significantly higher fusion of MDM into osteoclasts compared to non-infected cells (Ctrl:26.5±3.3; Wh:51.0±5.1; BA.5:52.3±7.5).
These findings demonstrate that SARS-CoV-2-enhanced osteoclastogenesis involves not only RANKL-dependent differentiation but also RANKL-independent mechanisms.

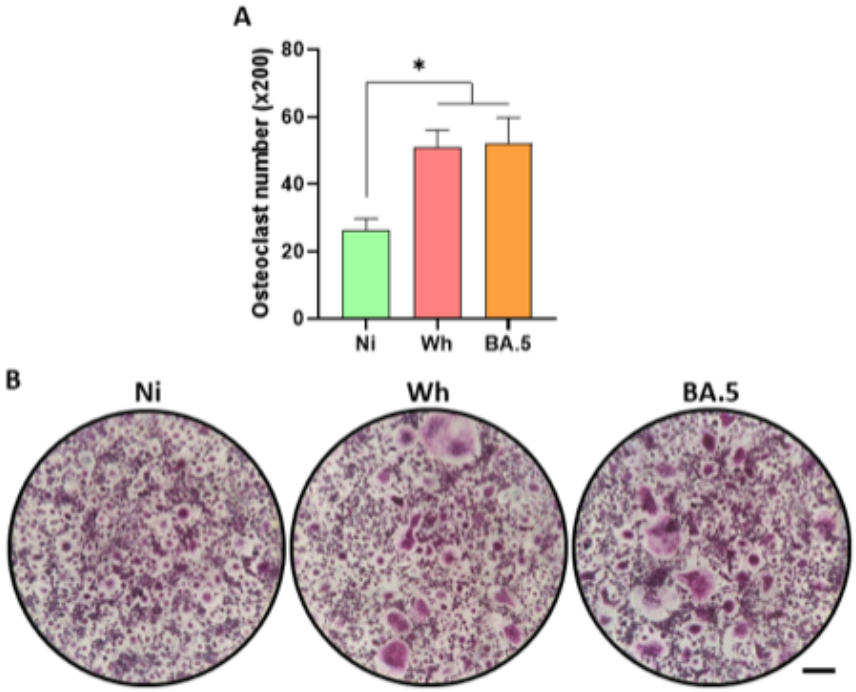

Figure 8. SARS-CoV-2-enhanced osteoclastogenesis through RANKL independent mechanism. **(A)** Quantifying the number of TRAP-positive osteoclasts (expressed as an absolute count) at 12 dpi in the absence of RANKL. **(B)** Representative images of (A) (x200). Ni, non-infected control. Wh, ancestral variant. BA.5, Omicron variant. Scale bar: 200 µm. *p < 0.05. n: 2-3 donors were used.

4. Discussion

In this investigation, despite causing an abortive infection in precursor macrophages of osteoclasts, the SARS-CoV-2's ability to accelerate osteoclastogenesis and bone resorption is highlighted. Limited studies on the direct impact of SARS-CoV-2 on osteoclast susceptibility and differentiation, primarily conducted in rodent models, have provided insights(16, 17, 22, 23). Studying SARS-CoV-2's impact on the skeletal system is challenging due to delayed onset, but lasting effects include bone metabolism disorders observed in COVID-19 patients(24, 25). Osteoclasts, originating from the monocyte/macrophage lineage (pre-OC), are exclusive bone-resorbing cells crucial for bone development and remodeling, actively contributing to musculoskeletal tissue damage. While consensus suggests that human monocyte-derived macrophages (MDMs) exposed to SARS-CoV-2 do not release infectious virions(20, 26-30), conflicting studies propose MDMs' potential support for initial infection stages, including viral entry, RNA replication, and protein synthesis(20, 26, 27, 30). Conversely, other research indicates MDM resistance to SARS-CoV-2 entry. Interestingly, despite their ability to support de novo synthesis of viral RNA and proteins, respiratory viruses like influenza A infect macrophages abortively(29).

In this study, utilizing both ancestral and Omicron strains, abortive infection of SARS-CoV-2 among human primary monocyte-derived macrophages (MDM), acting as pre-osteoclasts (pre-OCs) is demonstrated. This finding remains consistent despite a notable increase in ACE2 expression among pre-OC following exposure to SARS-CoV-2. A transient synthesis of viral RNA without de novo protein synthesis or virion release was observed. Early after the virus challenge, a pro-inflammatory cytokine profile, including TNF-α, IL-1β, and IL-6, was detected, gradually declining. Subsequently, SARS-CoV-2-exposed pre-OC exhibited increased transcriptional levels of anti-inflammatory cytokine genes (IL-10, TGF-β), elevated CD163 expression as a marker of inflammation resolution(31), and maintained cell viability. Morphological changes in pre-OC were noted, initially resembling an M1 profile, transitioning to an elongated cell reminiscent of the M2 macrophage profile(32). These morphological alterations, influenced by biophysical cues in the microenvironment, indicate the reversible repolarization capacity of macrophages(33). This observation aligns with previous reports of reversible repolarization in the context of *Cryptococcus neoformans* infection(34). The SARS-CoV-2-induced M1-to-M2 switch resulted in increased osteoclast differentiation, suggesting a higher bone-resorptive capacity(35). This M2-osteoclastogenic potential, associated with the silencing of factors enhancing M1 polarization, such as IRF5, highlights the intricate mechanisms by which SARS-CoV-2 modulates macrophage phenotypes and accelerates osteoclastogenesis(36).

Upon initiation of *in vitro* RANKL-induced osteoclastogenesis, a direct impact of SARS-CoV-2 abortive infection on pre-osteoclasts (pre-OCs) was observed, leading to a concurrent increase in osteoclastogenesis in a dose-dependent manner. Additionally, SARS-CoV-2 abortive infection prompted the formation of larger osteoclasts, significantly enhancing the expression of osteoclast-specific markers, including tartrate-resistant acid phosphatase and CD51/61, while also upregulating osteoclast bone resorption activity. Such findings further revealed elevated mRNA levels of inducible genes associated with osteoclast differentiation, such as RANK, NFATc1 (master regulator controlling genes like TRAP and MMP-9), and DC-STAMP (master fusogenic protein). The heightened mROS levels in SARS-CoV-2-exposed pre-OC correlated with an upregulated TNFα-mediated inflammatory response, characteristic of the initial M1 profile and crucial for M2 macrophage differentiation(37, 38). Remarkably, unlike other target cells such as epithelial, hepatocytes, and cholangiocytes, the redox balance and viability of abortively infected osteoclasts (OC) remained intact. This suggests the potential for these infected cells to persist for an extended period within bones.

These findings unveil an intriguing aspect: priming with transforming growth factor β (TGF-β) enables TNF-α to induce osteoclastogenesis effectively, bypassing the canonical RANKL pathway. This discovery holds significance as inflammatory cytokines, including TNF-α, typically have limited capacity to directly stimulate osteoclast differentiation. The production of TGF-β induced by SARS-CoV-2 transforms TNF-α's pro-inflammatory action on macrophages into a highly efficient osteoclastogenic function, creating a chromatin environment favorable for the expression of osteoclastic genes(39). Consequently, even in the absence of productive infection in osteoclast precursor cells, SARS-CoV-2 accelerates osteoclastogenesis through both RANKL-dependent and independent mechanisms.

In symptomatic COVID and even in patients who survive its initial stage but with persistent symptoms, often referred to as "long COVID" or "post-acute sequelae of SARS-CoV-2 infection" (PASC), arthralgia or rheumatic complaints are frequently reported (8, 40-42), but fewer efforts have been put forward to explore the underlying factors behind SARS-CoV-2-induced arthralgia.

This study has limitations. Firstly, the experiments primarily utilized peripheral blood mononuclear cells (PBMCs) from multiple donors, potentially introducing subtle differences between donors. However, the consistent and robust observations across multiple assays

validate the stimulatory effect of SARS-CoV-2 infection. Secondly, the current model relies on an isolated culture system, valuable for screening direct effects on the osteoclast phenotype. Nevertheless, these findings necessitate further validation in in vivo models. Thirdly, the observed phenotypic effects lack complete support from gene expression profiles, partly due to the chosen time point, inherent cell population heterogeneity, and concurrent expression of key markers. Future studies will focus on investigating these markers and their interactions at the protein level.

In summary, this study sheds light on the role of osteoclastogenesis in SARS-CoV-2 pathogenesis using a primary in vitro human model. This model enhances the understanding of the factors contributing to bone loss following SARS-CoV-2 infection. These findings reveal disruptions in osteoclast differentiation and function due to SARS-CoV-2 infection. An alternative mechanism driving bone pathology, which results in accelerated bone resorption, is proposed. This model presents potential targets for therapeutic and preventive interventions against SARS-CoV-2, especially concerning long-term complications associated with COVID-19.

Funding Statement

This work was supported by a grant from the Agencia Nacional de Promoción Científica y Tecnológica (ANPCYT, Argentina), PICTO 2021-COVID secuelas-00005 to JQ, and ILE. The funding agency had no role in the study design, data collection and analysis, decision to publish, or preparation of the manuscript.

Author Contributions

F.S. and P.J. performed the experiments and analyzed the data. C.C., R.N.F, and C.A.M.L helped with viral stocks and culture media preparation. J.C.G. performed western blots. J.Q. wrote the manuscript. J.Q., I.L.E, and M.V.D. designed the experiments, revised the manuscript, and obtained research funding. All authors have read and agreed to the published version of the manuscript.

Data Availability Statement

The raw data supporting the conclusions of this article will be made available by the authors, without undue reservation.

Conflicts of Interest

The authors declare no conflict of interest.

5. References

1. Gupta A, Madhavan MV, Sehgal K, Nair N, Mahajan S, Sehrawat TS, et al. Extrapulmonary manifestations of COVID-19. Nat Med. 2020;26(7):1017-32.
2. Chan JF, Yuan S, Kok KH, To KK, Chu H, Yang J, et al. A familial cluster of pneumonia associated with the 2019 novel coronavirus indicating person-to-person transmission: a study of a family cluster. Lancet. 2020;395(10223):514-23.
3. To KK, Sridhar S, Chiu KH, Hung DL, Li X, Hung IF, et al. Lessons learned 1 year after SARS-CoV-2 emergence leading to COVID-19 pandemic. Emerg Microbes Infect. 2021;10(1):507-35.
4. Carfi A, Bernabei R, Landi F, Gemelli Against C-P-ACSG. Persistent Symptoms in Patients After Acute COVID-19. JAMA. 2020;324(6):603-5.
5. Huang C, Huang L, Wang Y, Li X, Ren L, Gu X, et al. 6-month consequences of COVID-19 in patients discharged from hospital: a cohort study. Lancet. 2021;397(10270):220-32.

6. Sudre CH, Murray B, Varsavsky T, Graham MS, Penfold RS, Bowyer RC, et al. Attributes and predictors of long COVID. Nat Med. 2021;27(4):626-31.
7. Maffia-Bizzozero S, Cevallos C, Lenicov FR, Freiberger RN, Lopez CAM, Guano Toaquiza A, et al. Viable SARS-CoV-2 Omicron sub-variants isolated from autopsy tissues. Front Microbiol. 2023;14:1192832.
8. Davis HE, Assaf GS, McCorkell L, Wei H, Low RJ, Re'em Y, et al. Characterizing long COVID in an international cohort: 7 months of symptoms and their impact. EClinicalMedicine. 2021;38:101019.
9. Kottlors J, Grosse Hokamp N, Fervers P, Bremm J, Fichter F, Persigehl T, et al. Early extrapulmonary prognostic features in chest computed tomography in COVID-19 pneumonia: Bone mineral density is a relevant predictor for the clinical outcome - A multicenter feasibility study. Bone. 2021;144:115790.
10. Arai F, Miyamoto T, Ohneda O, Inada T, Sudo T, Brasel K, et al. Commitment and differentiation of osteoclast precursor cells by the sequential expression of c-Fms and receptor activator of nuclear factor kappaB (RANK) receptors. J Exp Med. 1999;190(12):1741-54.
11. Jacome-Galarza CE, Percin GI, Muller JT, Mass E, Lazarov T, Eitler J, et al. Developmental origin, functional maintenance and genetic rescue of osteoclasts. Nature. 2019;568(7753):541-5.
12. Shibakawa A, Yudoh K, Masuko-Hongo K, Kato T, Nishioka K, Nakamura H. The role of subchondral bone resorption pits in osteoarthritis: MMP production by cells derived from bone marrow. Osteoarthritis Cartilage. 2005;13(8):679-87.
13. Raynaud-Messina B, Bracq L, Dupont M, Souriant S, Usmani SM, Proag A, et al. Bone degradation machinery of osteoclasts: An HIV-1 target that contributes to bone loss. Proc Natl Acad Sci U S A. 2018;115(11):E2556-E65.
14. Sviercz FA, Jarmoluk P, Cevallos CG, Lopez CAM, Freiberger RN, Guano A, et al. Massively HIV-1-infected macrophages exhibit a severely hampered ability to differentiate into osteoclasts. Front Immunol. 2023;14:1206099.
15. Mumtaz N, Koedam M, van Leeuwen J, Koopmans MPG, van der Eerden BCJ, Rockx B. Zika virus infects human osteoclasts and blocks differentiation and bone resorption. Emerg Microbes Infect. 2022;11(1):1621-34.
16. Qiao W, Lau HE, Xie H, Poon VK, Chan CC, Chu H, et al. SARS-CoV-2 infection induces inflammatory bone loss in golden Syrian hamsters. Nat Commun. 2022;13(1):2539.
17. Awosanya OD, Dalloul CE, Blosser RJ, Dadwal UC, Carozza M, Boschen K, et al. Osteoclast-mediated bone loss observed in a COVID-19 mouse model. Bone. 2022;154:116227.
18. Gao J, Mei H, Sun J, Li H, Huang Y, Tang Y, et al. Neuropilin-1-Mediated SARS-CoV-2 Infection in Bone Marrow-Derived Macrophages Inhibits Osteoclast Differentiation. Adv Biol (Weinh). 2022;6(5):e2200007.
19. Schmittgen TD, Livak KJ. Analyzing real-time PCR data by the comparative C(T) method. Nat Protoc. 2008;3(6):1101-8.
20. Zheng J, Wang Y, Li K, Meyerholz DK, Allamargot C, Perlman S. Severe Acute Respiratory Syndrome Coronavirus 2-Induced Immune Activation and Death of Monocyte-Derived Human Macrophages and Dendritic Cells. J Infect Dis. 2021;223(5):785-95.
21. Choi HK, Kim TH, Jhon GJ, Lee SY. Reactive oxygen species regulate M-CSF-induced monocyte/macrophage proliferation through SHP1 oxidation. Cell Signal. 2011;23(10):1633-9.
22. Haudenschild AK, Christiansen BA, Orr S, Ball EE, Weiss CM, Liu H, et al. Acute bone loss following SARS-CoV-2 infection in mice. J Orthop Res. 2023;41(9):1945-52.
23. Queiroz-Junior CM, Santos A, Goncalves MR, Brito CB, Barrioni B, Almeida PJ, et al. Acute coronavirus infection triggers a TNF-dependent osteoporotic phenotype in mice. Life Sci. 2023;324:121750.
24. Yang C, Ma X, Wu J, Han J, Zheng Z, Duan H, et al. Low serum calcium and phosphorus and their clinical performance in detecting COVID-19 patients. J Med Virol. 2021;93(3):1639-51.

25. di Filippo L, Doga M, Frara S, Giustina A. Hypocalcemia in COVID-19: Prevalence, clinical significance and therapeutic implications. Rev Endocr Metab Disord. 2022;23(2):299-308.
26. Thorne LG, Reuschl AK, Zuliani-Alvarez L, Whelan MVX, Turner J, Noursadeghi M, et al. SARS-CoV-2 sensing by RIG-I and MDA5 links epithelial infection to macrophage inflammation. EMBO J. 2021;40(15):e107826.
27. Abdelmoaty MM, Yeapuri P, Machhi J, Olson KE, Shahjin F, Kumar V, et al. Defining the Innate Immune Responses for SARS-CoV-2-Human Macrophage Interactions. Front Immunol. 2021;12:741502.
28. Dalskov L, Mohlenberg M, Thyrsted J, Blay-Cadanet J, Poulsen ET, Folkersen BH, et al. SARS-CoV-2 evades immune detection in alveolar macrophages. EMBO Rep. 2020;21(12):e51252.
29. Labzin LI, Chew KY, Eschke K, Wang X, Esposito T, Stocks CJ, et al. Macrophage ACE2 is necessary for SARS-CoV-2 replication and subsequent cytokine responses that restrict continued virion release. Sci Signal. 2023;16(782):eabq1366.
30. Niles MA, Gogesch P, Kronhart S, Ortega Iannazzo S, Kochs G, Waibler Z, et al. Macrophages and Dendritic Cells Are Not the Major Source of Pro-Inflammatory Cytokines Upon SARS-CoV-2 Infection. Front Immunol. 2021;12:647824.
31. Evans BJ, Haskard DO, Sempowksi G, Landis RC. Evolution of the Macrophage CD163 Phenotype and Cytokine Profiles in a Human Model of Resolving Inflammation. Int J Inflam. 2013;2013:780502.
32. Sun Y, Li J, Xie X, Gu F, Sui Z, Zhang K, et al. Macrophage-Osteoclast Associations: Origin, Polarization, and Subgroups. Front Immunol. 2021;12:778078.
33. Sica A, Mantovani A. Macrophage plasticity and polarization: in vivo veritas. J Clin Invest. 2012;122(3):787-95.
34. Davis MJ, Tsang TM, Qiu Y, Dayrit JK, Freij JB, Huffnagle GB, et al. Macrophage M1/M2 polarization dynamically adapts to changes in cytokine microenvironments in Cryptococcus neoformans infection. mBio. 2013;4(3):e00264-13.
35. Yang J, Park OJ, Kim J, Kwon Y, Yun CH, Han SH. Modulation of macrophage subtypes by IRF5 determines osteoclastogenic potential. J Cell Physiol. 2019;234(12):23033-42.
36. Cords L, Woost R, Kummer S, Brehm TT, Kluge S, Schmiedel S, et al. Frequency of IRF5+ dendritic cells is associated with the TLR7-induced inflammatory cytokine response in SARS-CoV-2 infection. Cytokine. 2023;162:156109.
37. Tan HY, Wang N, Li S, Hong M, Wang X, Feng Y. The Reactive Oxygen Species in Macrophage Polarization: Reflecting Its Dual Role in Progression and Treatment of Human Diseases. Oxid Med Cell Longev. 2016;2016:2795090.
38. Zhang Y, Choksi S, Chen K, Pobezinskaya Y, Linnoila I, Liu ZG. ROS play a critical role in the differentiation of alternatively activated macrophages and the occurrence of tumor-associated macrophages. Cell Res. 2013;23(7):898-914.
39. Xia Y, Inoue K, Du Y, Baker SJ, Reddy EP, Greenblatt MB, et al. TGFbeta reprograms TNF stimulation of macrophages towards a non-canonical pathway driving inflammatory osteoclastogenesis. Nat Commun. 2022;13(1):3920.
40. Mohammadian Erdi A, Zakavi M, Amani M, Fooladi S, Abedi A. Clinical manifestations of pain in patients suffering from COVID-19 infected with Delta variant of SARS-Cov-2. Front Pain Res (Lausanne). 2023;4:1282527.
41. Hoshijima H, Mihara T, Seki H, Hyuga S, Kuratani N, Shiga T. Incidence of long-term post-acute sequelae of SARS-CoV-2 infection related to pain and other symptoms: A systematic review and meta-analysis. PLoS One. 2023;18(11):e0250909.
42. Alexander AJ, Joshi A, Mehendale A. The Musculoskeletal Manifestations of COVID-19: A Narrative Review Article. Cureus. 2022;14(9):e29076.